doi:10.1016/j.jmb.2007.02.071 J. Mol. Biol. (2007) 368, 1087–1100

JMB

Available online at www.sciencedirect.com

ScienceDirect

ELSEVIER

DEAD-box-protein-assisted RNA Structure Conversion Towards and Against Thermodynamic Equilibrium Values

Quansheng Yang[1], Margaret E. Fairman[1] and Eckhard Jankowsky[1,2]*

[1]*Department of Biochemistry School of Medicine, Case Western Reserve University Cleveland, OH 44106, USA*

[2]*Center for RNA Molecular Biology, School of Medicine Case Western Reserve University, Cleveland OH 44106, USA*

**Corresponding author*

RNAs in biological processes often interconvert between defined structures. These RNA structure conversions are assisted by proteins and are frequently coupled to ATP hydrolysis. It is not well understood how proteins coordinate RNA structure conversions and which role ATP hydrolysis has in these processes. Here, we have investigated *in vitro* how the DEAD-box ATPase Ded1 facilitates RNA structure conversions in a simple model system. We find that Ded1 assists RNA structure conversions *via* two distinct pathways. One pathway requires ATP hydrolysis and involves the complete disassembly of the RNA strands. This pathway represents a kinetically controlled steady state between the RNA structures, which allows formation of less stable from more stable RNA conformations and thus RNA structure conversion against thermodynamic equilibrium values. The other pathway is ATP-independent and proceeds *via* multi-partite intermediates that are stabilized by Ded1. Our results provide a basic mechanistic framework for protein-assisted RNA structure conversions that illuminates the role of ATP hydrolysis and reveal an unexpected diversity of pathways.

Keywords: DEAD-box; helicase; RNA structure; ATPase; RNA chaperone

Introduction

RNAs in biological processes such as pre-mRNA splicing, ribosome biogenesis, RNA export, and translation have to fold into distinct structures and often interconvert between defined structures in an accurate and exquisitely timed fashion.[1,2] Examples of such RNA structure conversions (also called conformational switches[1]) from the pre-mRNA splicing machinery include the exchange of U1 for U6, the disruption of U4/U6 stem II and subsequent formation of U6 3′ stem–loop, and the disruption of the U2 5′ stem–loop and subsequent formation of the U2/U6 helix II.[2] Many, if not all RNA structure conversions are assisted by proteins,[1,2] but it is unclear which roles proteins have in complex RNA re-arrangements. For example, interconverting RNA structures are often mutually exclusive, i.e. one RNA structure has to be disrupted to form another one,[2] but it is not understood how proteins facilitate the necessary RNA re-arrangements in an accurate and well-timed fashion. In addition, more stable RNA structures are frequently converted into less stable conformations.[2] While this is a potentially important distinction to processes that govern the folding of functional RNAs, which generally occurs from unfolded *via* less stable to more stable conformations,[3,4] it is uncertain how RNA structures can be converted against thermodynamic equilibrium values and how proteins assist in such reactions.

One group of proteins pivotal for facilitating RNA structure conversions are the DExH/D proteins, the largest group of enzymes in eukaryotic RNA metabolism.[5] DExH/D proteins are highly conserved, with at least eight characteristic sequence motifs.[6] The sequence of the characteristic motif II provides the name DExH/D, in the single letter code. DExH/D proteins remodel RNA structure or RNA–protein interactions in an ATP-dependent fashion.[7,8] Although it is not known where precisely the vast majority of DExH/D proteins bind to their targets or which exact conformational changes these proteins catalyze in their respective substrates, physiological

Abbreviations used: FRET, fluorescence energy transfer; TIR, total internal reflection; PEG, polyethylene glycol.

E-mail address of the corresponding author: exj13@case.edu

functions of many DExH/D proteins correlate with their ability to hydrolyze ATP in an RNA-stimulated manner, and often with the ability of the enzymes to unwind RNA duplexes *in vitro* in an ATP-dependent fashion. For these reasons, DExH/D proteins are frequently referred to as RNA helicases and, as such, are implicated mainly in steps involving the disassembly of RNA complexes. However, several DEAD-box proteins, (motif II takes the form DEAD, DEAD-box proteins are the largest DExH/D protein subfamily[7]) have been shown recently to facilitate the formation of RNA duplexes, in addition to their ability to unwind those.[9,10] These observations suggested that the function of certain DEAD-box proteins may not be restricted to the disruption of RNA duplexes or RNA protein interactions, but that these enzymes perhaps utilize both, unwinding and annealing activities to directly assist RNA structure conversions.[9] While this is an attractive prospect, given the involvement of some DEAD-box proteins in physiological RNA structure conversions,[2,9] including the splicing of group I and group II introns,[11,12] it is unknown how DEAD-box proteins may coordinate complex structural changes in an RNA.

To understand how DEAD-box proteins facilitate RNA structure conversions, relevant reactions have to be analyzed quantitatively. It is presently not technically possible to quantitatively dissect physiological RNA structure conversions because those usually occur within large RNA–protein complexes, such as the splicing machinery, which cannot be controlled easily *in vitro*. However, progress in the knowledge of protein and RNA folding demonstrates that mechanistic principles of complex conformational rearrangements can be illuminated by investigating defined and tractable model systems.[4,13]

Here, we have devised a simple model system that recapitulates essential aspects of RNA structure conversions such as the mutually exclusive nature of the structures formed. With this system, we have investigated how the DEAD-box protein Ded1 facilitates complex structural changes in RNA *in vitro*. Ded1 is an essential enzyme from *Saccharomyces cerevisiae* that has been shown to unwind and anneal RNA duplexes.[10,14–16] Here, we show that Ded1 can assist RNA structure conversions *via* two distinct pathways. One pathway requires ATP hydrolysis and allows the formation of less stable RNA structures from more stable structures, i.e. a distribution of RNA structures against thermodynamic equilibrium values. The second pathway does not involve ATP hydrolysis and proceeds *via* the stabilization of an intermediate comprised of components from both RNA structures. This pathway does not allow RNA structure conversions against thermodynamic equilibrium values, and resembles reactions catalyzed by proteins with RNA chaperone activity. Collectively, our results provide a basic mechanistic framework for protein-assisted RNA conversions that illuminates a role for ATP hydrolysis and reveals an unexpected diversity of pathways.

Results

Substrate design

To investigate Ded1-facilitated RNA structure conversions, we designed a tripartite RNA system (strands *x*, *y*, and *z*, Figure 1(a)). As the physiological RNA targets of Ded1 are not known, the sequence of the RNA strands was not based on a specific biological RNA system. In our tripartite RNA model system, strand *y* formed a stable structure with either strand *z* (complex *A*) or strand *x* (complex *B*) (Figure 1(a)). That is, formation of complex *A* required disruption of complex *B*, and *vice versa*.

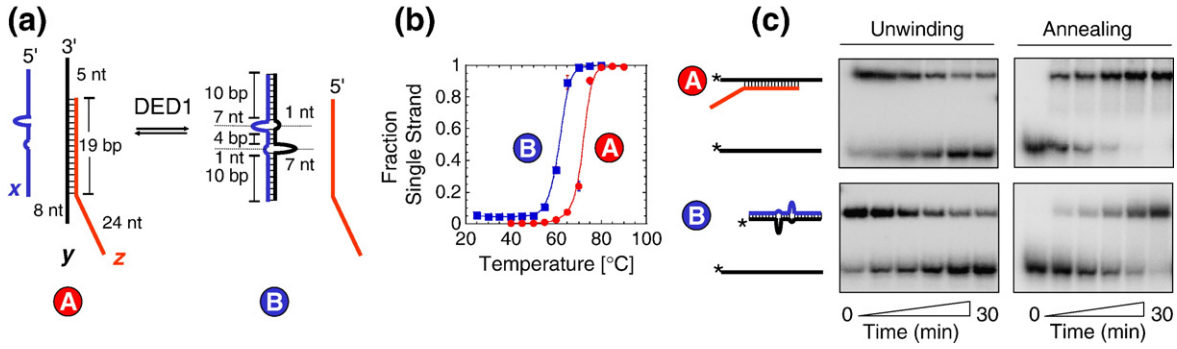

Figure 1. Substrate design and characterization. (a) Substrate design. Three single strands (*x*, *y*, *z*) form two mutually exclusive structures (*A* and *B*). Numbers indicate the base-pairs formed, and the unpaired nucleotides. (b) Thermal melting curves of structures *A* and *B*. The curves represent a smoothed trend, yielding a melting temperature for complex *A* of $T_m^A = 75.0(\pm 0.5)$ °C and a melting temperature for complex *B* of $T_m^B = 65.0(\pm 0.5)$ °C. (c) Representative gels for ATP-dependent unwinding of *A* and *B* (two left panels), and facilitation of strand annealing for both complexes (two right panels) by Ded1. Unwinding reactions were performed with 0.5 mM ATP at 24 °C. The average unwinding rate constants from multiple independent experiments were $k_{unw}^{\mathbf{A}} = 1.1(\pm 0.2)$ min^{-1} and $k_{unw}^{\mathbf{B}} = 2.1(\pm 0.2)$ min^{-1}. Annealing reactions were performed in the absence of ATP at 24 °C. Average annealing rate constants from multiple independent experiments were $k_{ann}^{\mathbf{A}} = 6.0(\pm 0.8)\cdot 10^9$ M^{-1}min^{-1} and $k_{ann}^{B} = 2.8(\pm 0.5)\cdot 10^9$ M^{-1}min^{-1}. Strand annealing without Ded1 yielded less than 5% product in 30 min (data not shown).

Further considerations for the design of the RNA substrates included: (i) distinct thermodynamic stability of both substrates; (ii) ability of Ded1 to completely bind both RNA structures at experimentally accessible enzyme concentrations; (iii) ability of Ded1 to unwind both structures with rate constants allowing manual monitoring of the reaction; (iv) ability of Ded1 to facilitate the formation of complexes out of the single strands; and (v) marked separation of both structures from each other and from single-stranded RNA on PAGE.

Complex *B* had a lower thermodynamic stability than complex *A*. At 0.5 nM RNA, the melting temperature for *B* was lower than that of *A* by 10 deg.C (Figure 1(b)). The stability difference was maintained with Ded1 bound; Ded1 bound to complex *A* with a higher affinity (K_d = 17(±2) nM) than to complex *B* (K_d = 208(±17) nM, data not shown). Both *A* and *B* were unwound by Ded1 in an ATP-dependent fashion, and the enzyme facilitated the formation of both structures out of single strands (Figure 1(c)).

RNA structure conversion by Ded1

To measure the extent to which Ded1 could convert complex *A* into complex *B*, and *vice versa*, it was necessary to determine the distribution of the two structures at the thermodynamically controlled equilibrium under the respective reaction conditions. To this end, pre-formed *A* was combined with strand *x*. The mixture was heated to 95 °C and cooled slowly to the reaction temperature, which allowed the two structures to form in a distribution dictated by thermodynamic stabilities and respective concentrations (Figure 2(a)). The resulting distribution of the RNA complexes was analyzed by non-denaturing PAGE and yielded a distribution of 20% *B* and 80% *A* (Figure 2(a), lane Δ*T*). An identical distribution was detected when strand *z* was added to pre-formed *B* (identical concentrations), indicating that 20% *B* and 80% *A* indeed reflected equilibrium values (data not shown). Thus, as expected, the thermodynamic equilibrium between the two RNA structures favored formation of the more stable *A* over *B* by a factor of 4 at the reaction conditions and the concentrations used.

We then tested whether the two RNA structures could interconvert without a protein co-factor (Figure 2(b)). Starting with 100% *A*, no notable conversion to *B* was detected within 6 h (Figure 2(b)). No conversion of *B* into *A* was seen when pre-formed *B* (100%) was incubated with strand *z* at concentrations and conditions identical with those used for the reverse reaction. Thus, without protein co-factors, no RNA structure conversion was observed within the reaction time.

Addition of Ded1 without ATP resulted in a clearly measurable conversion of complex *A* into *B* (Figure 2(c)). Starting at 100% *A*, approximately 20% *A* were converted into *B*, upon which the reaction reached a steady level virtually identical with the distribution between complexes *A* and *B* dictated by the thermodynamic equilibrium (i.e. 20% *B*, 80% *A*, Figure 2(a)). Starting the reaction with pre-formed *B* (100%), and free strand *z*, resulted in the same distribution between *A* (80%) and *B* (20%) (Figure 2(c)). These observations preclude the possibility that the levels of *B* and *A* were caused by formation of a dead-end complex. Rather, the data indicated that Ded1, in the absence of ATP, had the capacity to facilitate the RNA structure conversion by accelerating the observed rate constant for establishing the thermodynamic equilibrium between the two RNA structures.

Next, we measured the conversion of *A* to *B* by Ded1 in the presence of ATP (Figure 2(d)). This reaction proceeded significantly faster than the structure conversion without ATP. Moreover, an amplitude was reached at 60% *B* (Figure 2(d)). This level of *B* is clearly above the 20% *B* seen in both the reaction by Ded1 without ATP and in the establishment of the thermodynamic equilibrium between the two structures. Thus, Ded1 with ATP appeared to be able to convert the more stable into the less stable RNA structure. Conversion of *B* into *A* with Ded1 and ATP also yielded 60% *B* and 40% *A*, a distribution identical with that seen in the reverse reaction (Figure 2(d)). This observation, again, precluded formation of dead-end complexes as a possible reason for the measured distribution. ATP alone did not facilitate any measurable structure conversion (data not shown). The non-hydrolysable ATP analog AMPPNP, which has been shown to bind to Ded1,[10,16] could not substitute for ATP (data not shown). Therefore, hydrolysis and not mere ATP binding were critical for the observed structure conversion. Collectively, these data indicated that Ded1, in the presence of ATP, can establish a distribution between RNA structures favoring the less stable conformation. In addition, the RNA structure conversion occurs markedly faster with than without ATP.

To further probe the role of ATP hydrolysis, we tested the effect of ATP depletion during the reaction (Figure 2(e)). To this end, conversion of *A* (100%) to *B* with Ded1 and ATP was allowed to proceed for ten minutes, after which the reaction amplitude of 60% *B* was reached (Figure 2(e), lane S). Then hexokinase was added,[17] which hydrolyzed the ATP in the reaction mix within approximately 4 s (ATP decay data not shown). We observed a clear decrease of the fraction *B*, accompanied by an increase in the fraction of *A* (Figure 2(e)). This transition reached a plateau at 20% *B* and 80% *A*, the distribution dictated by the thermodynamic equilibrium value. This result indicates that continuous ATP hydrolysis by Ded1 is required to maintain a *B*/*A* distribution shifted towards the less stable structure.

To explore correlations between the concentration of ATP and the Ded1-mediated structure conversion process, we performed reactions in the presence of a higher concentration of ATP (0.5 mM, Figure 2(f)). The distribution of *B* and *A* in the steady state was not significantly different from that at the lower concentration of ATP (0.1 mM, Figure 2(d)). How-

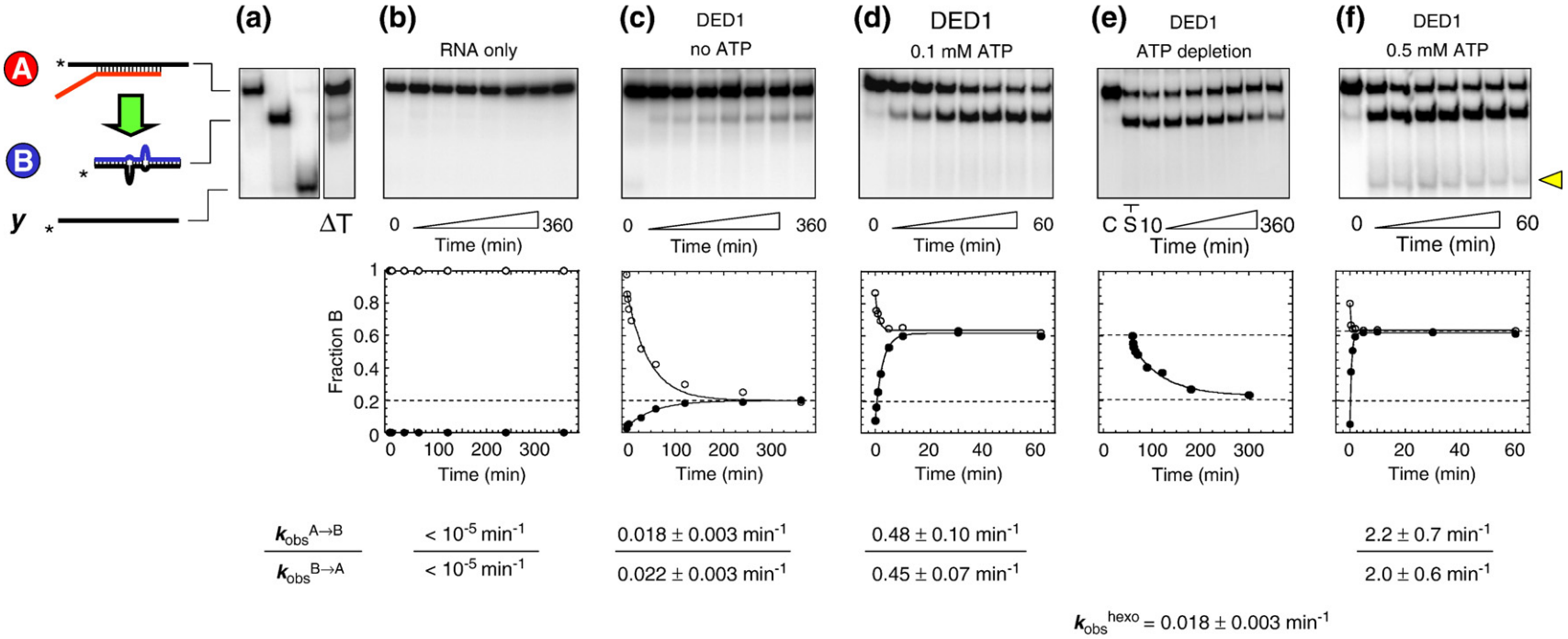

Figure 2. RNA structure conversions. (a) Size standards (left panel) and thermodynamically dictated equilibrium between structures A and B (right panel, Δ*T*). Cartoons indicate species *A*, *B*, and strand *y*, the asterisk represents the radiolabel. The green block arrow emphasizes that reactions were started with pre-formed complex *A*. The procedure to measure the thermal equilibrium is described in Materials and Methods. (b)–(f) Representative time-courses for structure conversion (*A*→*B*) (●), and for the reverse reaction, *B*→*A* (○). Aliquots were removed as indicated underneath the gels. Plots below the gel panels show time-courses for structure conversion *A*→*B* (●), and for the reverse reaction, *B*→*A* (○). The fraction of complex B (Fraction B) is plotted *versus* time. Fraction B was calculated from the amount of radioactivity in the bands representing species *A*, *B*, and *y*, according to Fraction B = B/(A + B + y). The dotted lines indicate the distribution between structures *A* (80%) and *B* (20%) at the thermodynamically dictated equilibrium, and the distribution in the presence of Ded1 and ATP (*A* 40%, *B* 60%). Lines represent the best fit to the integrated form of a homogeneous first-order rate law. Observed first-order rate constants (k_{obs}) were computed from multiple independent experiments and are listed under the plots. The fit of plot of the time-course after hexokinase addition (e) lists the observed rate constant (k_{obs}^{hexo}) for the transition from distribution of the ATP-dependent steady state to the thermodynamic equilibrium. The triangle in (f) indicates the single-stranded species *y*.

ever, the reaction proceeded significantly faster at the higher concentration of ATP, indicating that more energy "consumed" during the reaction affected primarily the reaction kinetics and less the distribution between the RNA structures (discussed in more detail below).

We also noted a slight, yet significant accumulation of single-stranded RNA *y* (Figure 2(f), triangle). A further rise in the concentration of ATP resulted in an even larger fraction of this single-stranded species (Figure 3(a)). At 2 mM ATP, approximately 80% of the RNA was single-stranded (Figure 3(b)).

Basic kinetic mechanism for ATP-dependent RNA structure conversion

The accumulation of single-stranded species at higher concentrations of ATP suggested that the RNA structure conversion involved ATP-dependent duplex unwinding by Ded1 (Figure 3). From the disassembled strands, the actual structure conversion could then be accomplished readily by the ability of Ded1 to promote strand annealing.[10] The strand annealing activity does not require ATP, and the rate constant for the annealing steps do not change at lower concentrations of ATP as markedly as the rate constants for the disassembly steps.[10] Therefore, it seemed likely that at lower concentrations of ATP, virtually all disassembled strands reacted immediately, further forming the new structure (Figure 4(a)). Consistent with previous observations,[10] the rate constants for the strand separations increased with the concentration of ATP, whereas the rate constants for the annealing steps decreased more markedly at higher concentrations of ATP (Figure 4(b)). As a consequence, the disassembly of the strands is favored at higher concentrations of ATP, and single-stranded species accumulate.

The simple two-step process (Figure 4(a)) quantitatively explained the distribution between *A* and *B* against the thermodynamic equilibrium value, the relative insensitivity of the distribution at concentrations of ATP between 0.1 mM and 0.5 mM (Figure 4(c)), and the observed accumulation of single-stranded species only at higher concentrations of ATP (Figure 4(d)). Rate constants obtained by the fit closely matched the respective rate constants determined separately for unwinding and annealing reactions of the respective complexes (Figure 1(c)). We concluded that this basic two-step mechanism was therefore sufficient to quantitatively explain our observations during RNA structure conversions with ATP.

This kinetic model shows Ded1 facilitating RNA structure conversions through the establishment of a kinetically controlled, ATP hydrolysis-dependent steady state between the two RNA structures. The kinetics of disassembly and formation of the RNA structures, rather than their thermodynamic stabilities determine the distribution of the complexes. It is interesting to note that the distribution of *B*/*A* is not determined solely by the unwinding rate constants, as this scenario would have yielded Fraction $B = 0.35$ in the steady state (still favoring the less stable structure more than the thermodynamically controlled equilibrium with Fraction $B = 0.2$). The observed distribution, Fraction $B = 0.6$, thus indicates that the ability of Ded1 to facilitate both duplex unwinding and strand annealing is critical for the structure conversion. The relatively constant ratio of rate constants for unwinding and annealing steps dictates the largely unchanged A/B ratio at 0.1 mM and 0.5 mM ATP, yet the structure conversion occurs faster at higher concentrations of ATP.

ATP-independent structure conversion proceeds *via* tripartite species

While the mechanism described above explained the structure conversion with ATP, it remained unclear how Ded1 facilitated the reaction without ATP. Clearly, depletion of ATP during the reaction changed the distribution of *A* and *B* (Figure 2(e)). Furthermore, Ded1 was unable to unwind either RNA complex without ATP within the time-frame of our experiments (data not shown). Especially, the latter observation precluded a mechanism for the ATP-independent structure conversion proceeding

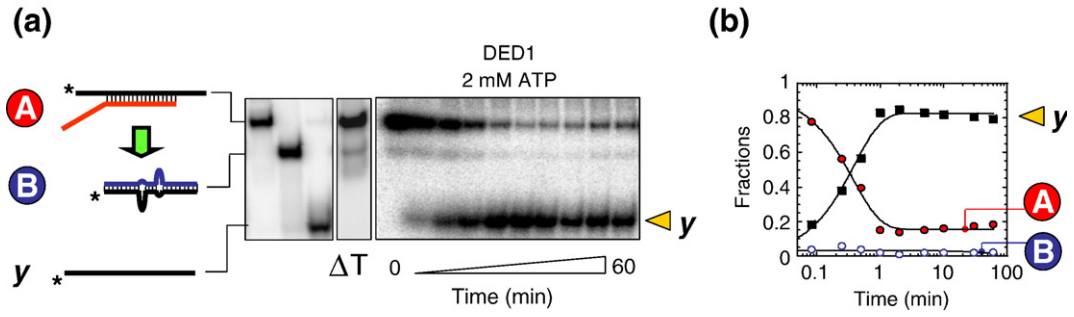

Figure 3. RNA structure conversion with Ded1 and 2 mM ATP. (a) Size standards and representative time-course of a structure conversion (*A*→*B*) with Ded1 in the presence of 2 mM ATP. Cartoons indicate species *A*, *B*, and strand *y* (triangle). The asterisk represents the radiolabel. Reactions were performed with 0.5 nM A and 2 mM *x*, to emphasize the emergence of the single-stranded *y*. (b) Plot of a representative time-course for conversion *A*→*B* with 2 mM ATP. Species *A*, *B*, and strand *y* are plotted as indicated. Note the logarithmic scale of the time axis. Lines represent the best fit to the integrated form of a homogeneous first-order rate law. The apparent rate constant for emergence of strand *y* is $k^{y}_{unw} = 2.3(\pm 0.3)\ min^{-1}$.

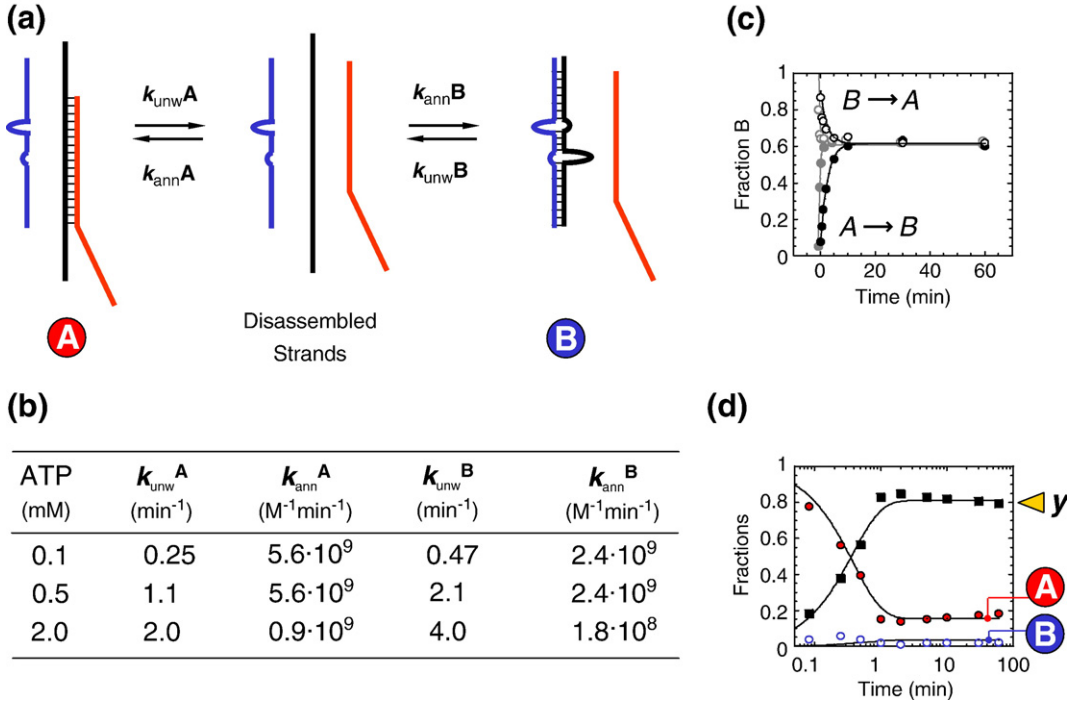

(b)

ATP (mM)	k_{unw}^{A} (min^{-1})	k_{ann}^{A} ($M^{-1}min^{-1}$)	k_{unw}^{B} (min^{-1})	k_{ann}^{B} ($M^{-1}min^{-1}$)
0.1	0.25	$5.6 \cdot 10^9$	0.47	$2.4 \cdot 10^9$
0.5	1.1	$5.6 \cdot 10^9$	2.1	$2.4 \cdot 10^9$
2.0	2.0	$0.9 \cdot 10^9$	4.0	$1.8 \cdot 10^8$

Figure 4. Basic kinetic scheme for structure conversion with Ded1 and ATP. (a) Schematics for the reaction. (b) Rate constants for individual reaction steps at different concentrations of ATP. Rate constants were determined by numerically fitting the time-courses shown in Figures 2 and 3 using the Kinsim/Fitsim software package.[35] (c) Simulated time-courses (lines) using these rate constants for 0.5 mM ATP (gray) and 0.1 mM ATP (black) for both structure conversions $A \rightarrow B$ (●), and $B \rightarrow A$ (○). The points included represent actual data. (d) Simulated time-course for the reaction in the presence of 2 mM ATP, species *A*, *B*, and *y* are plotted as indicated.

via disassembled strands. If the strands were not disassembled, then the only other pathway in our tripartite system would require intermediates containing all three RNA strands in one complex.

To probe the existence of such tripartite RNA species, we employed a fluorescence technique (Figure 5(a)). We labeled strand *x* with Cy5 and strand *z* with Cy3, two fluorophores that undergo fluorescence energy transfer (FRET), when within a distance of less than approximately 8 nm.[18] A tripartite RNA species was thus expected to yield a FRET signal (Figure 5(a)). When Cy3-labeled complex *A* was incubated with only Cy5-labeled strand *x*, no FRET was observed (Figure 5(b), left panel), suggesting no significant accumulation of an eventual tripartite intermediate. However, addition of Ded1 without ATP resulted in a small, yet significant FRET signal (Figure 5(b), middle panel). The FRET signal was strictly dependent on the presence of strand *y*. Omitting this strand under otherwise identical conditions produced no FRET in the presence of Ded1 (Figure 5(c) and (d)). The observed FRET therefore suggested a genuine tripartite species, not a Ded1-mediated aggregation of the strands *z* and *x*.

Addition of 0.5 mM ATP decreased the FRET signal between *A* and strand *x*, compared to the reaction without ATP (Figure 5(b), right panel), and the FRET signal disappeared at higher concentrations of ATP (data not shown). These results are consistent with the above finding, that Ded1 disassembled the RNA strands in the presence of ATP. FRET signals similar to those described above were observed when Cy5-labeled complex *B* was incubated with Cy3-labeled strand *z* and Ded1 in the absence of ATP (data not shown). Thus, the Ded1-facilitated formation of tripartite species was not restricted to strand *x* associating with complex *A*. Rather, a tripartite species could be formed as soon as an RNA region was available that allowed the pairing of a few bases.

However, the low FRET signal raised the question of whether the tripartite intermediate was stable or formed only transiently. A low FRET signal could be caused by a highly populated (stable) state with low FRET efficiency, or by a rarely populated (unstable) state with high FRET efficiency.[19–21] To distinguish between these two possibilities, we conducted fluorescence measurements at the single-molecule level (Figure 6). We used the labeling scheme described above and a wide-field, total internal reflection (TIR)-based single molecule fluorescence detection system (see Materials and Methods).[20] Cy3-labeled complex *A* was immobilized and free, Cy5-labeled strand *x* was present in solution (Figure 6(a)). As in the ensemble measurement above, Cy3-labeled complex *A* was expected to show no FRET signal, whereas the tripartite should produce a higher FRET value.

In the presence of Ded1 without ATP, time trajectories of individual complexes showed long durations without FRET (FRET ~ 0) punctuated by short spikes of high FRET (FRET ~ 1, Figure 6(b)). Without Ded1, only the low FRET state was observed

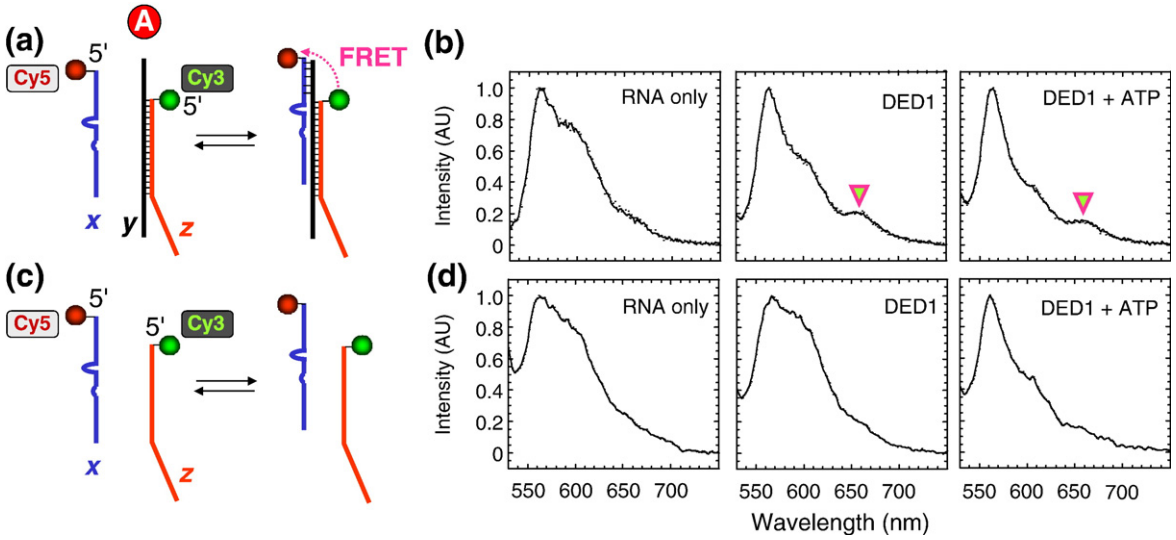

Figure 5. Ded1-assisted stabilization of tripartite intermediate. (a) Position of the fluorescent labels. Cy3 is indicated by a green circle (on complex *A*, strand *z*), and Cy5 by a red circle on strand *x*. (b) Ensemble fluorescence spectra. Preformed complex *A* (Cy3) was incubated with strand *x* (Cy5) in the absence of Ded1 and ATP (left panel), with Ded1 (middle panel), and with Ded1 and 0.1 mM ATP (right panel). The triangle indicates the emission resulting from energy transfer of the tripartite complex. The FRET intensity in the presence of Ded1 without ATP (middle panel) is ~0.04, as estimated by fitting of the spectra with three Gaussian curves and analysis of the areas corresponding to donor and acceptor emission after normalization to the spectra in the absence of Ded1. The FRET intensity with ATP (right panel) is ~0.02. (c) Control reactions without strand *y*. (d) Ensemble fluorescence spectra without strand *y*. Strand *x* (Cy3) was incubated with strand *z* (Cy5) in the absence of Ded1 and ATP (left panel), with Ded1 (middle panel), and with Ded1 and 0.1 mM ATP (right panel). Concentrations were as in (b).

and no FRET spike was detected in any of the time trajectories (data not shown). These observations suggested immediately that in the presence of Ded1, the tripartite species were present for only short times. Analysis of FRET values for all recorded spikes revealed that the FRET for the majority of these spikes was high, although there was a smaller population of spikes with intermediate FRET values, which may indicate multiple distinct tripartite species (Figure 6(c)). However, a histogram of durations of the FRET spikes fit well to a single-exponential decay with a lifetime of $\tau = 0.17(\pm 0.02)$ s, (Figure 6(d)), indicating that a possible heterogeneity was without marked consequence for the stability of the respective tripartite species. We note that the time-resolution of the instrument (10 fps) precluded accurate recording of events shorter than 0.1 s, and many FRET spikes lasted for only one frame. Therefore, the lifetime of the tripartite species of $\tau = 0.17$ s should be viewed as an upper limit. Nonetheless, our data demonstrate clearly that the FRET spikes were universally short. These results, in conjunction with the ensemble fluorescence data, indicate that without ATP, Ded1 transiently stabilizes one or several tripartite intermediates that are otherwise too fragile to accumulate.

With ATP (0.5 mM), Ded1 caused a significant decrease in the number of immobilized complexes *A* over the course of a few minutes (data not shown). These observations are consistent with the ability of Ded1 to unwind complex *A* in an ATP-dependent fashion (Figure 1(c)). In no case were the unwinding events accompanied by an increase in FRET, strongly supporting the conclusion that, in the presence of ATP, Ded1 completely disassembled the RNA strands without formation of tripartite intermediates. Time trajectories for Cy3-labeled complex *A* before unwinding events, however, were highly similar to those without ATP (data not shown). We concluded that these time trajectories showed Ded1 without ATP bound, given the sub-saturating concentrations of ATP. These observations are in excellent agreement with the ensemble FRET measurements, which showed a lower average FRET in the presence of these sub-saturating concentrations of ATP (Figure 5(b), right panel).

With Ded1 but in the absence of ATP, we also observed a small number of time trajectories (approximately 10 in 10^4 overall trajectories) where complexes, after reaching the high FRET state, did not return immediately to the low FRET state, but continued to show prolonged fluorescence fluctuations (Figure 7). These time trajectories are consistent with a scenario where a tripartite complex does not immediately dissociate but reacts further towards the complete structure conversion (Figure 7(a)). The fluorescence fluctuations may reflect movement of the fluorescently labeled strands *x* and *z* back and forth on strand *y*, much like a branch migration (Figure 7(b)). The distinct signature of these time trajectories thus suggested that the observed tripartite species are on-pathway for the structure conversion. The small number of time trajectories showing these distinct prolonged fluorescence fluctuations precluded a sound statistical analysis, and effects other than the scenario discussed above may there-

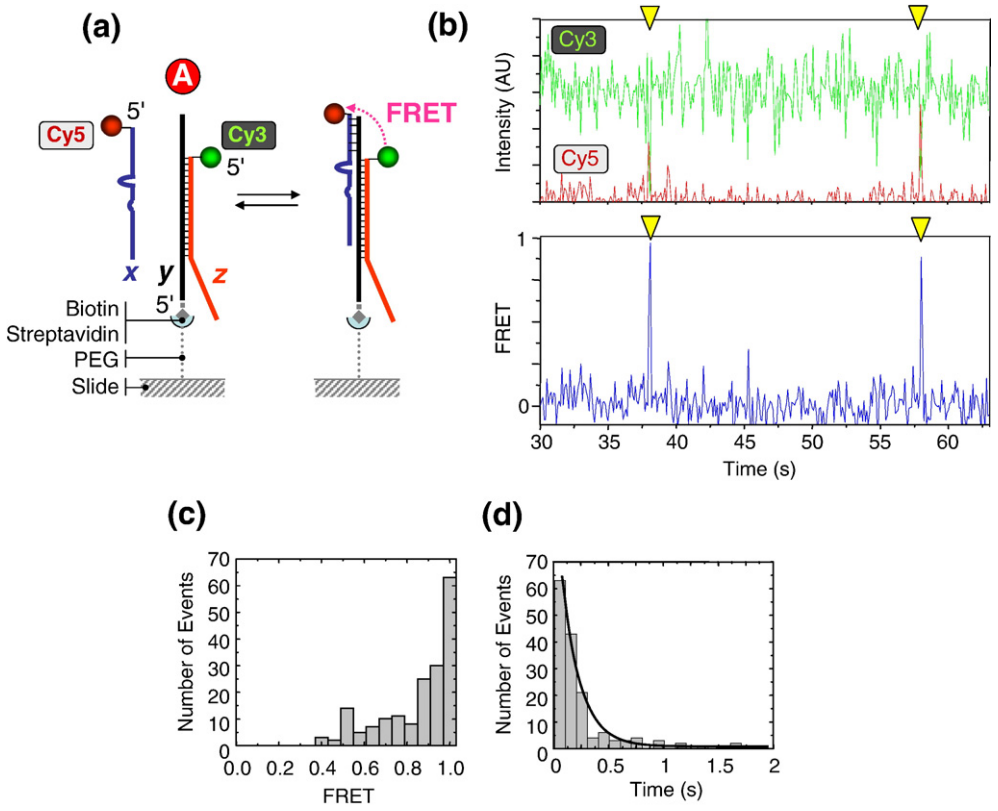

Figure 6. Transient formation of tripartite species detected at the single molecule level. (a) Immobilization of fluorescently labeled complex *A via* biotinylated strand *y*. The complex was immobilized *via* a streptavidin link to a quartz slide coated with polyethylene glycol to prevent non-specific binding of the protein to the slide.[35] Cy5-labeled strand *x* was present in solution at 8 nM. (b) Representative time-trace of an individual complex *A* in the presence of Ded1 and Cy5-labeled strand *x* (upper panel). The yellow triangles emphasize the short, anti-correlated spikes of high Cy5 and low Cy3 intensity, indicative of the transient formation of tripartite species. The lower panel shows the above time-trace converted to FRET intensity according to: FRET = intensity(acceptor)/(intensity(acceptor) + intensity(donor)) with intensities corrected for channel crosstalk.[21] (c) Histogram of the FRET intensity of multiple anti-correlated spikes. The FRET intensity given in the left panel represents the average FRET value of the individual spikes, regardless of their duration. (d) Statistical analysis of the duration of the high FRET spikes. The duration of individual FRET spikes was measured with a customized Matblab program.[20] The dwell time of molecules in the high FRET state (>0.6) is plotted in the histogram. The line represents a fit of the data points to a single-exponential decay, yielding $\tau = 0.17(\pm 0.02)$ s and thus a rate constant by which strand *x* dissociates from the tripartite intermediate of $k_{\mathrm{diss}}^{(x)} = 353(\pm 41)\ \mathrm{min}^{-1}$.

fore account for the observations. However, a small number of complete structure conversion events observed in single-molecule trajectories is consistent with the ensemble kinetics of the reaction, as discussed below.

Basic kinetic mechanism for ATP-independent RNA structure conversion

The fluorescence data described above established the brief existence of tripartite RNA species in the presence of Ded1 without ATP. Furthermore, the results suggested that the observed tripartite species may be on-pathway for the structure conversion without ATP. It is important to note that our results do not provide unambiguous proof for the latter assertion. The structure conversion may proceed through other tripartite complexes not detected in our measurements, or even *via* multiple pathways. However, the Ded1-assisted structure conversion without ATP involves tripartite species in any event, because the reaction cannot proceed through complete disassembly of the strands, as in the presence of ATP. Structure conversion without tripartite intermediates would require complete disassembly of *A* (or *B*) with a rate constant of at least $k_{\mathrm{unw}} > 0.02\ \mathrm{min}^{-1}$, the observed rate constant for the structure conversion without ATP (Figure 2). No comparable unwinding rate constant was detected when incubating complex *A* with Ded1 in the absence of ATP (data not shown). It is important to note that the detected tripartite species are not necessarily representing a homogeneous population, although eventual heterogeneity appears to be without marked consequence for the observed stability of the tripartite species.

Considering the caveats mentioned above, we propose a basic mechanism for the Ded1-assisted RNA structure conversion without ATP, on the basis of both fluorescence data and measurements of the RNA structure conversions by PAGE. The structure conversion proceeds through tripartite intermediates that are formed only transiently (Figure 8(a)).

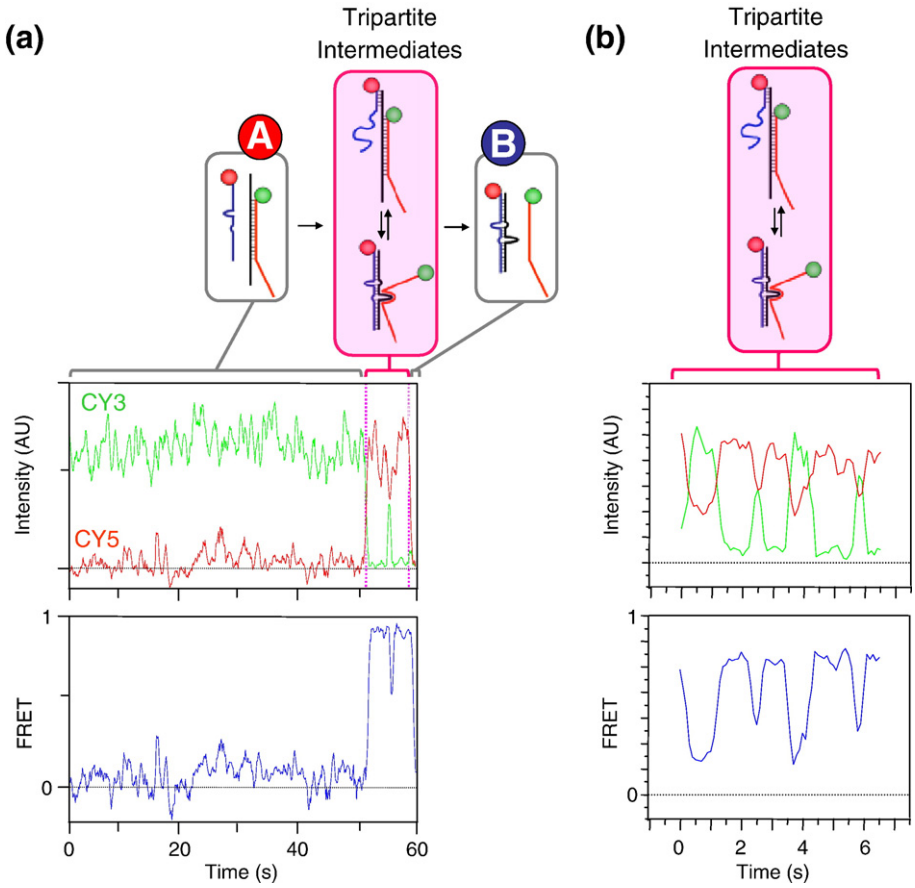

Figure 7. Persistent fluorescence fluctuations during the Ded1-assisted structure conversion without ATP. (a) Representative time-trace of a putative complete structure conversion. At ~51 s, the tripartite intermediate is formed, one distinct fluctuation is observed (~55 s), which may represent a back and forth migration of the two RNA structures. A decrease in overall fluorescence intensity is seen at ~59 s. This event is consistent with a final dissociation of strand *z*, which bears the Cy3 label. However, photo-deactivation of the Cy3 label might also account for this observation. The cartoons above illustrate the different states in the time-trace. The representation of the tripartite intermediates is speculative. (b) Representative time-trace for a putative tripartite species showing multiple FRET fluctuations. Only the fluorescence fluctuations are shown.

The lower limit for the dissociation rate constants of the tripartite species is reflected in the lifetime of the tripartite complexes, as measured with single-molecule FRET. Corresponding association rate constants were estimated from the FRET value seen in the ensemble measurements (FRET ~ 0.04, Figure 5(b)). Although numerous events indicating formation of tripartite species were observed directly in single-molecule experiments, it remains less clear how the physical transition from a tripartite species to the final structure *B* (and *A*) occurs. Most likely, a mechanism resembling a branch migration switches the structures from a tripartite species to the final complex (*B* or *A*). Presumably, a further opening of the existing helix during the short lifetime of the tripartite species could promote the respective RNA structures to "equilibrate" according to the thermodynamic stability of the respective complexes.

The number of trajectories showing prolonged fluctuations that presumably reflect such branch migration events, was small. However, the kinetic mechanism implies a slow step between the tripartite species and, therefore, the small number of trajectories showing the actual structure exchange is expected. According to the kinetic mechanism, the tripartite species should dissociate approximately 1000 times until one complete structure conversion occurs, which is consistent with the observations.

Regardless of the exact physical events leading to the strand exchange, the mechanism shown for the ATP-independent structure conversion *via* tripartite intermediates accounted quantitatively for the observed timecourses for reactions starting from *A* or *B* (Figure 8(b)). In addition, the mechanism accurately described the transition from the ATP-induced steady state towards the thermodynamic equilibrium upon sudden ATP depletion (Figure 2, simulation data not shown), and the mechanism accounted for all observations made during the fluorescence measurements.

Discussion

In this work, we used a tripartite model system to investigate an RNA structure conversion that is

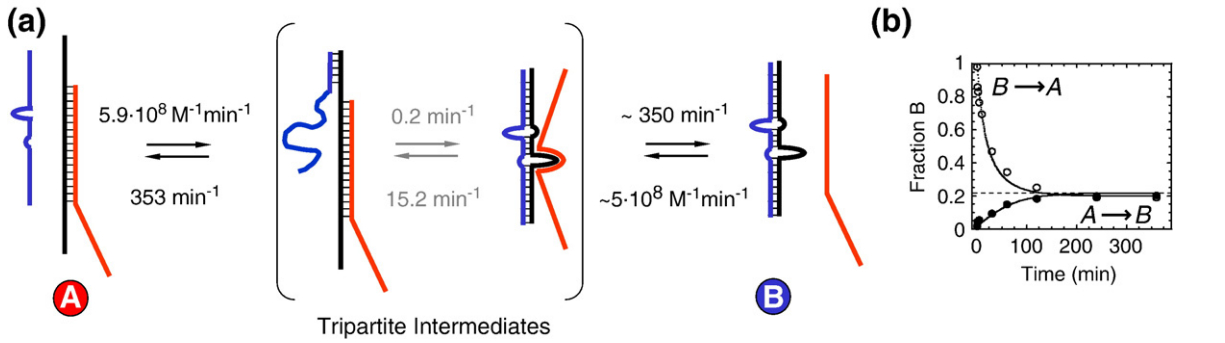

Figure 8. Basic kinetic scheme for Ded1-assisted structure conversion without ATP. (a) Rate constants for dissociation of strands *x* and *z* from the respective tripartite intermediates were determined with single-molecule experiments described for Figures 6 and 7. Data for dissociation of *z* are not shown. Corresponding association constants (strand *x* and complex *A*, and strand *z* and complex *B*) were determined from the equilibrium between complexes *A* and *B*, and the corresponding tripartite intermediates measured in ensemble FRET experiments (Figure 5). Data for ensemble FRET experiments of complex *B* with strand *z* are not shown. Rate constants for the actual strand exchange reaction (grey) were determined by numerically fitting time-courses in Figure 2 using the Kinsim/Fitsim software package.[35] Association and dissociation rate constants determined separately (black numbers) were fixed and the strand exchange rate constants were allowed to float. (b) Simulated time-courses (lines) using the rate constants given in (a) for both structure conversions $A \rightarrow B$ (●), and $B \rightarrow A$ (○). The points included represent actual data.

assisted by the DEAD-box protein Ded1. Despite its simplicity, the model system recapitulates essential aspects of much more complex physiological structure conversions, notably the mutually exclusive nature of the two RNA structures, and the conversions towards, and, for the first time shown *in vitro*, against thermodynamic equilibrium values. The basic mechanistic features elucidated in this work may thus also underlie more complex protein-assisted RNA structure conversions.

We have found that the Ded1-assisted RNA structure conversion can proceed *via* two distinct pathways, depending on whether ATP is present (Figure 9). The pathway without ATP involves multipartite intermediates and results in a distribution of the RNA structures dictated by thermodynamic equilibrium values. The ATP-dependent pathway proceeds *via* completely disassembled RNA structures and allows RNA structure conversion against thermodynamic equilibrium values. Without Ded1, none of the two possible pathways for RNA structure conversion can be sufficiently populated within the reaction time.

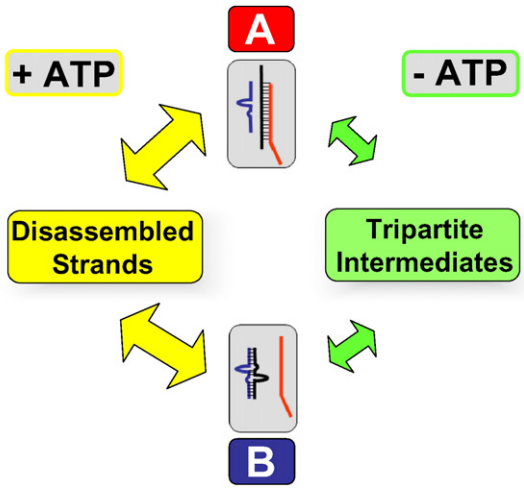

Figure 9. DED- assisted RNA structure conversion. Schematics of the ATP-dependent (left) and the ATP-independent (right) pathway of the structure conversion. Complexes and intermediates are labeled as in the preceding text and Figures. The different sizes of the arrows indicate the distinct observed rate constants for the respective reactions.

If Ded1 is present without ATP, no strand separation can be detected, which precludes a structure conversion *via* disassembled strands with the observed kinetics. Therefore, in a system comprising only three strands, the structure conversion must proceed through species with all three strands in one complex. We have observed these tripartite species directly (Figures 5–7). While it remains unclear whether these complexes represent one or multiple species, it is evident that the tripartite complexes are stabilized by Ded1. Nevertheless, even with Ded1, the tripartite species still dissociate with rate constants exceeding $k_{diss} > 300$ min^{-1} (Figure 6). Yet, for approximately 1000 dissociation events now roughly one transition from one structure to the other (e.g. A→B) can occur. This small probability is sufficient to enable the interconversion of the two RNA structures within the reaction time.

We have observed several single-molecule trajectories that presumably show complete structure conversions (Figure 7). These trajectories suggest that the structure conversion proceeds from the observed tripartite intermediates, placing these species on-pathway" for the structure conversion. Only a small fraction of the trajectories (~0.1% of all observed traces) show these complete structure conversions, which precludes a sound statistical analysis of these processes. Nonetheless, it is critical to note that the ensemble kinetics indicate such a small number of complete structure conversions relative to the number of events showing formation

and dissociation of tripartite species. Thus, all of our observations made with various techniques can be explained quantitatively with the proposed kinetic model (Figure 8).

Notwithstanding, we note that it is formally possible that the observed tripartite species are not on-pathway for the actual structure conversion, because processes involved in the exchange of the structures *A* to *B* could be completely invisible to our fluorescence assays. Given the geometry of the complex and the labeling scheme, which should detect dyes as far apart as ~80 Å,[21] we consider this possibility somewhat unlikely. In any event, for the reasons mentioned above, the structure conversion in the absence of Ded1 must still proceed through tripartite species.

Our observations leave open the question of how exactly the transition between tripartite intermediates and final RNA structures takes place. The data appear most consistent with a process resembling a branch migration, starting perhaps from the region that allows base-pairing between all three strands. As discussed above, several single-molecule trajectories presumably show such putative branch migration events (Figure 7). Our data do not indicate whether Ded1 (without ATP) accelerates the putative branch migration process, but we note that branch migrations can occur spontaneously, as has been observed in other systems.[22,23]

Irrespective of the actual mode of transition from the tripartite species to the final RNA structure, our results suggest that RNA structure conversions can be facilitated through stabilization of inherently unstable RNA species. While stabilization of the weak RNA–RNA interactions by proteins may be important throughout RNA metabolism,[1,2,24–26] such structure stabilization has never been observed directly for a DEAD-box protein. Nonetheless, stabilization of tripartite species by Ded1 may correlate with the capacity of the enzyme to facilitate strand annealing.[10] In fact, acceleration of strand annealing by a protein may be based on the stabilization of inherently unstable species that form during the rate-limiting steps of duplex formation.[25,27] Therefore, a protein scoring in an annealing assay could in fact function to stabilize inherently unstable RNA structures, which may explain why RNA-binding proteins often facilitate strand annealing.[1,28]

As the pathway for the Ded1-facilitated RNA structure conversion without ATP involves only equilibrium binding steps, the final distribution of the RNA structures is dictated by the thermodynamic equilibrium value. In this respect, this structure conversion pathway resembles strand-exchange reactions by proteins with RNA chaperone activity, such as Ncp7.[29,30] These RNA chaperones also produce a ratio of RNA structures dictated by thermodynamic equilibrium values.[1,28] Most proteins with RNA chaperone activity have significant annealing activities, which, as discussed above, may correlate with a capacity to stabilize inherently unstable RNA species. It is thus attractive to speculate that other proteins with RNA chaperone activity may facilitate RNA structure conversions *via* the stabilization of tripartite intermediates, although this remains to be shown.

If Ded1 is present with ATP, the structure conversion proceeds *via* complete disassembly of the strands, which requires ATP-hydrolysis (Figure 9). Subsequently, Ded1 uses its annealing activity to reform the other duplex. This pathway constitutes a kinetically controlled steady state between unwinding and annealing reactions: the ratio between the RNA structures is determined solely by the rate constants for unwinding and annealing reactions, not by the thermodynamic stability of the structures. Thus, Ded1 can facilitate an RNA structure conversion against thermodynamic equilibrium values. To our knowledge, this is the first time such a process has been demonstrated directly *in vitro*. Continuous ATP hydrolysis by Ded1 is necessary to maintain a ratio of RNA structures against their thermodynamic equilibrium values.

While the ATP-driven, kinetic steady state between the RNA structures always results in a distribution of the RNA structures that differs from the distribution dictated by thermodynamic equilibrium values, higher concentrations of ATP favor the strand separation reactions and thus result in an accumulation of single-stranded species. It is interesting to note that within a certain range of ATP concentrations (in our system between 0.1 mM and 0.5 mM, Figure 2), the amount of ATP hydrolyzed, while affecting the reaction kinetics, may impact the distribution of the RNA species in the steady state only slightly.

The RNA structure conversion pathway *via* an ATP-driven, kinetically controlled steady state shows a simple means by which a distribution of RNA structures can be maintained independent of thermodynamic equilibrium values. In other systems, rate constants for strand separation and annealing as well as RNA concentrations will clearly differ, and thus RNA structure distributions will be different too, yet the same basic mechanism for such helicase-driven, ATP-dependent RNA structure conversions will most likely apply.

The data presented here also illuminate features advantageous for proteins functioning in RNA structure conversions. Proteins working without ATP would be efficient when they stabilize tripartite intermediates to a high degree and/or if they accelerate the subsequent "branch migration". Proteins employing ATP hydrolysis would be particularly efficient if the strand separation step is fast, although this rate constant would perhaps need to be coordinated with the subsequent strand annealing. Otherwise, single-stranded species would accumulate, which may or may not be problematic. However, the ATP-dependent pathway may be significantly faster than the ATP-independent pathway. Thus, employing ATP-driven RNA unwinding activities in addition to annealing activities for RNA structure conversions allows RNA structure conversions against thermodynamic equilibrium values and allows those reactions to

occur fast. Potentially, fast structure conversions allow better timed conformational changes in RNPs.

Materials and Methods

Materials

Ded1 was expressed in *Escherichia coli* and purified as described.[31] RNA oligonucleotides were purchased from DHARMACON. Hexokinase was purchased from ROCHE. Radiolabeling of the oligonucleotides, and formation and purification of complexes *A* and *B* was performed as described.[32] Sequences were as follows:

strand *x*: 5′-CCGUACAGACAUUGCACCUGGCG-CUGUCUGGG,
strand *y*: 5′-CCCAGACAGCAUUGUACCCAGAGU-CUGUACGG,
strand *z*: 5′-CAGACUCUGGGUACAAUGCACGUA-CUAACAGCAUCAAUGACAU.

Fluorescently labeled and biotinylated oligonucleotides were purchased from DHARMACON. Fluorophores were attached at the 5′ end of strands *x*, and *z*, as indicated in Figures 5 and 6. Biotin, where applicable, was attached at the 5′ end of strand *y* (Figure 6). The extent of labeling was assessed by UV spectroscopy and found to be greater than 80% according to extinction coefficients of the RNA and the fluorophores.

Thermal melting curves

Melting temperatures of complexes *A* and *B* were determined in reaction buffer containing 40 mM Tris–HCl (pH 8.0), 50 mM NaCl, 0.5 mM $MgCl_2$, 2 mM DTT, 1 unit/μl of RNasin, 0.01% (v/v) NP40. Complexes (*A* or *B*) at 0.5 nM were incubated at the indicated temperatures ranging from 24 °C to 95 °C in a temperature-calibrated PCR machine for 5 min. Then reactions were transferred onto ice in buffer containing 1% (w/v) SDS, 50 mM EDTA, 0.1% (w/v) xylene cyanol, 0.1% (w/v) bromophenol blue, 20% (v/v) glycerol. Subsequently, aliquots were submitted to a non-denaturing PAGE (15% (w/v) polyacrylamide gel), duplex and single-stranded RNAs were separated, and the fraction of single-stranded RNAs were determined and plotted *versus* incubation temperature (Figure 1 (b)).

Unwinding and annealing reactions

Reactions were performed as described[10] at 24 °C, in a volume of 20 μl in a buffer containing 40 mM Tris–HCl (pH 8.0), 50 mM NaCl, 0.5 mM $MgCl_2$, 2 mM DTT, 1 unit/μl of RNasin, 0.01% NP40. RNA complexes and single strands, where applicable, were present at 0.5 nM, Ded1 was present at 800 nM. Rate constants for unwinding and annealing reactions were calculated as described.[10]

Structure conversion reactions

Reactions were performed at 24 °C in a volume of 30 μl in a buffer containing 40 mM Tris–HCl (pH 8.0), 50 mM NaCl, 0.5 mM $MgCl_2$, 2 mM DTT, 1 unit/μl of RNasin, 0.01% NP40. Unless stated otherwise, for the conversion of structure *A* into *B*, 2 nM pre-formed complex *A* and 8 nM-strand *x* (final concentrations) were used; for the conversion of structure *B* into *A*, 2 nM pre-formed complex *B*, and 6 nM strand *x* and 2 nM strand *z* were used, in order to maintain equal concentrations of all individual strands (*x*, *y*, and *z*) in all reactions. Complex and single-stranded RNAs at these concentrations were incubated for 5 min at the reaction temperature. The reactions were initiated by addition of 800 nM Ded1 and an equimolar mixture of ATP and $MgCl_2$ at the concentrations indicated. Higher concentrations of Ded1 did not alter the observed kinetics, indicating that Ded1 was present at saturating concentrations. In the reactions with ATP, ADP accumulation over the reaction time did not exceed 5% of the ATP starting concentration (data not shown). At these concentrations, the effects of ADP on the overall reaction are insignificant.[10]

Protein storage buffer was added to the reactions without Ded1. At the times indicated, 3 μl aliquots were removed and reactions were terminated on ice with 3 μl of stop buffer containing 1% SDS, 50 mM EDTA, 0.1% (w/v) xylene cyanol, 0.1% (w/v) bromophenol blue, 20% (v/v) glycerol. Subsequently, aliquots were submitted to non-denaturing PAGE.[33] Gels were dried and bands corresponding to single-stranded and complex RNAs were visualized and quantified with a PhosphorImager (Molecular Dynamics). The percentages of complexes *A* and *B* given in the text are the percentages of the respective complexes relative to all labeled species.

The distribution of the complexes *A* and *B* at the thermodynamically dictated equilibrium (Figure 2 (a)) was determined by incubating either 2 nM pre-formed complex *A* and 8 nM of strand *x* (final concentrations), and, in an alternative reaction, 2 nM pre-formed complex *B*, and 6 nM strand *x* and 2 nM strand *z* at 95 °C for 2 min in reaction buffer and subsequent cooling of the respective mixture to the reaction temperature over 120 min. The mixture was then treated as described above, i.e. placed on ice, combined with stop buffer and sumitted to non-denaturing PAGE.

Ensemble fluorescence measurements

In a SPEX Fluoromax 2 fluorimeter, Cy5-labeled strand *x* was incubated with 10 nM Cy3-labeled complex *A* in the reaction buffer given above. Where applicable, 800 nM Ded1 and/or an equimolar mixture of ATP and $MgCl_2$ (at the concentrations indicated) was included. Reactions were incubated for 5 min (incubation times of up to 30 min were tested and did not alter the results) and then Cy3 was excited at a wavelength of 515 nm (5 nm). Fluorescence emission was measured from 530 nm to 750 nm (5 nm increments).

Single-molecule fluorescence measurements

Single-molecule fluorescence was measured in a home-built TIR microscope setup. The system is analogous to that described by Zhuang *et al*.[20] Core components include a Nikon TE300 microscope, Pentamax Gen III CCD (Princeton Instruments), and a 50 mW, frequency doubled solid-state laser (Crystalaser). Samples (50 pM Cy3-labeled complex *A*) were immobilized in a flow-cell coated with polyethylene glycol (PEG) to prevent non-specific protein absorption.[18,34] Briefly, a mixture of PEG-NHS (3000–5000 Da) and biotinylated PEG-NHS (3000 Da) (SHEARWATER) was covalently attached to the flow-cells that

were amino-functionalized with Vectabond (VECTOR). Biotinylated samples were immobilized through streptavidin (MOLECULAR PROBES) to the biotinylated PEG.[18,34] Non-specific binding of the labeled RNA complex, which was tested by omission of streptavidin, was found to be less than 5% of the specific binding. Molecules were immobilized at an average distance of at least 2–3 μm between individuals, i.e. at multiples of the diffraction limit. Photobleaching studies confirmed that more than 90% of the fluorescent spots corresponded to single fluorophores. Control reactions measuring Ded1-RNA binding verified that inactivation of Ded1 under the conditions of the single-molecule experiments was insignificant (data not shown).

Reactions were conducted in the buffer used for the above experiments, except that 5% (v/v) glucose was added together with an oxygen-scavenging system consisting of glucose oxidase (SIGMA) and catalase (SIGMA).[20] Control reactions confirmed that these conditions did not affect the reaction kinetics in solution significantly (data not shown). Samples were excited by TIR (532 nm) and the fluorescence was collected through a 60×, 1.2 N.A. water immersion objective (NIKON). Excitation light was blocked with a 550 nm long-path filter (OMEGA). Donor and acceptor fluorescence images were split by a dichroic filter (650 nm, OMEGA) and the two resulting paths were projected onto one half of the CCD, respectively. Control reactions showed that individual complexes (other RNA complexes showing high FRET with Cy5/Cy3 labels) were photostable under the reaction and measurement conditions for more than 30 s (data not shown). Single-molecule time traces were collected at a rate of 10 fps using customized software.[20] Fluorescence and corresponding FRET values were computed as described.[20] Data analysis was performed with customized Matlab routines.[20]

Acknowledgements

We thank Drs Anna Marie Pyle, Mike Harris, and Mark Caprara for comments on the manuscript. We are grateful to Dr Peter deHaseth for the opportunity to use the fluorimeter. This work was supported by a grant from the NIH (GM067700) to E.J.

References

1. Schroeder, R., Barta, A. & Semrad, K. (2004). Strategies for RNA folding and assembly. *Nature Rev. Mol. Cell Biol.* **5**, 908–919.
2. Staley, J. P. & Guthrie, C. (1998). Mechanical devices of the spliceosome: motors, clocks, springs, and things. *Cell*, **92**, 315–326.
3. Russell, R., Zhuang, X., Babcock, H. P., Millett, I. S., Doniach, S., Chu, S. & Herschlag, D. (2002). Exploring the folding landscape of a structured RNA. *Proc. Natl Acad. Sci. USA*, **99**, 155–160.
4. Lilley, D. M. (2005). Structure, folding and mechanisms of ribozymes. *Curr. Opin. Struct. Biol.* **15**, 313–323.
5. Tanner, N. K. & Linder, P. (2001). DExD/H box RNA helicases. From generic motors to specific dissociation functions. *Mol. Cell*, **8**, 251–261.
6. Jankowsky, E., Fairman, M. E. & Yang, Q. (2005). RNA helicases: versatile ATP-driven nanomotors. *J. Nanosci. Nanotechnol.* **12**, 1983–1989.
7. Rocak, S. & Linder, P. (2004). DEAD-box proteins: the driving forces behind RNA metabolism. *Nature Rev. Mol. Cell Biol.* **5**, 232–241.
8. Bowers, H. A., Maroney, P. A., Fairman, M. E., Kastner, B., Luehrmann, R., Nilsen, T. W. & Jankowsky, E. (2006). Discriminatory RNP remodeling by the DEAD-box protein DED1. *RNA*, **12**, 903–912.
9. Cordin, O., Banroques, J., Tanner, N. K. & Linder, P. (2006). The DEAD-box protein family of RNA helicases. *Gene*, **367**, 17–37.
10. Yang, Q. & Jankowsky, E. (2005). ATP- and ADP-dependent modulation of RNA unwinding and strand annealing activities by the DEAD-box protein DED1. *Biochemistry*, **44**, 13591–13601.
11. Solem, A., Zingler, N. & Pyle, A. M. (2006). A DEAD protein that activates intron self-splicing without unwinding RNA. *Mol. Cell*, **24**, 611–617.
12. Halls, C., Mohr, S., Del Campo, M., Yang, Q., Jankowsky, E. & Lambowitz, A. M. (2007). Involvement of DEAD-box proteins in group I and group II Intron Splicing. biochemical characterization of Mss116p, ATP hydrolysis-dependent and -independent mechanisms, and general RNA chaperone activity. *J. Mol. Biol.* **365**, 835–855.
13. Thirumalai, D. & Hyeon, C. (2005). RNA and protein folding: common themes and variations. *Biochemistry*, **44**, 4957–4970.
14. Linder, P. (2003). Yeast RNA helicases of the DEAD-box family involved in translation initiation. *Biol. Cell*, **95**, 157–167.
15. Iost, I., Dreyfus, M. & Linder, P. (1999). Ded1p, a DEAD-box protein required for translation initiation in *Saccharomyces cerevisiae*, is an RNA helicase. *J. Biol. Chem.* **274**, 17677–17683.
16. Yang, Q. & Jankowsky, E. (2006). The DEAD-box protein Ded1 unwinds RNA duplexes by a mode distinct from translocating helicases. *Nature Struct. Mol. Biol.* **13**, 981–986.
17. Rolland, F., Winderickx, J. & Thevelein, J. M. (2002). Glucose-sensing and -signalling mechanisms in yeast. *FEMS Yeast Res.* **2**, 183–201.
18. Ha, T. (2001). Single-molecule fluorescence resonance energy transfer. *Methods*, **25**, 78–86.
19. Zhuang, X. & Rief, M. (2003). Single-molecule folding. *Curr. Opin. Struct. Biol.* **13**, 88–97.
20. Zhuang, X., Bartley, L. E., Babcock, H. P., Russell, R., Ha, T., Herschlag, D. & Chu, S. (2000). A single-molecule study of RNA catalysis and folding. *Science*, **288**, 2048–2051.
21. Ha, T. (2001). Single-molecule fluorescence methods for the study of nucleic acids. *Curr. Opin. Struct. Biol.* **11**, 287–292.
22. McKinney, S. A., Tan, E., Wilson, T. J., Nahas, M. K., Declais, A. C., Clegg, R. M. *et al.* (2004). Single-molecule studies of DNA and RNA four-way junctions. *Biochem. Soc. Trans.* **32**, 41–45.
23. McKinney, S. A., Freeman, A. D., Lilley, D. M. & Ha, T. (2005). Observing spontaneous branch migration of Holliday junctions one step at a time. *Proc. Natl Acad. Sci. USA*, **102**, 5715–5720.
24. Weeks, K. M. & Cech, T. R. (1996). Assembly of a ribonucleoprotein catalyst by tertiary structure capture. *Science*, **271**, 345–348.
25. Eguchi, Y. & Tomizawa, J. (1990). Complex formed by complementary RNA stem-loops and its stabilization by a protein: function of CoIE1 Rom protein. *Cell*, **60**, 199–209.

26. Schroeder, R., Grossberger, R., Pichler, A. & Waldsich, C. (2002). RNA folding in vivo. *Curr. Opin. Struct. Biol.* **12**, 296–300.
27. Eckardt, S., Romby, P. & Sczakiel, G. (1997). Implications of RNA structure on the annealing of a potent antisense RNA directed against the human immunodeficiency virus type 1. *Biochemistry*, **36**, 12711–12721.
28. Rajkowitsch, L., Semrad, K., Mayer, O. & Schroeder, R. (2005). Assays for the RNA chaperone activity of proteins. *Biochem. Soc. Trans.* **33**, 450–456.
29. Cristofari, G. & Darlix, J. L. (2002). The ubiquitous nature of RNA chaperone proteins. *Prog. Nucl. Acid Res. Mol. Biol.* **72**, 223–268.
30. Urbaneja, M. A., Wu, M., Casas-Finet, J. R. & Karpel, R. L. (2002). HIV-1 nucleocapsid protein as a nucleic acid chaperone: spectroscopic study of its helix-destabilizing properties, structural binding specificity, and annealing activity. *J. Mol. Biol.* **318**, 749–764.
31. Fairman, M., Maroney, P. A., Wang, W., Bowers, H. A., Gollnick, P., Nilsen, T. W. & Jankowsky, E. (2004). Protein displacement by DExH/D RNA helicases without duplex unwinding. *Science*, **304**, 730–734.
32. Jankowsky, E., Gross, C. H., Shuman, S. & Pyle, A. M. (2000). The DExH protein NPH-II is a processive and directional motor for unwinding RNA. *Nature*, **403**, 447–451.
33. Jankowsky, E., Gross, C. H., Shuman, S. & Pyle, A. M. (2001). Active disruption of an RNA-protein interaction by a DExH/D RNA helicase. *Science*, **291**, 121–125.
34. Rasnik, I., McKinney, S. A. & Ha, T. (2005). Surfaces and orientations: much to FRET about? *Accts Chem. Res.* **38**, 542–548.
35. Zimmerle, C. T. & Frieden, C. (1989). Analysis of progress curves by simulations generated by numerical integration. *Biochem. J.* **258**, 381–387.

Edited by D. E. Draper

(Received 7 December 2006; received in revised form 30 January 2007; accepted 19 February 2007)
Available online 2 March 2007